

# Hydrodechlorination of Trichloroethylene to Hydrocarbons Using Bimetallic Nickel–Iron Nanoparticles

Bettina Schrick, Jennifer L. Blough, A. Daniel Jones, and Thomas E. Mallouk\*

Department of Chemistry, The Pennsylvania State University,  
University Park, Pennsylvania 16802

Received July 12, 2002. Revised Manuscript Received October 8, 2002

High surface-area nickel–iron nanoparticles (1:3 Ni:Fe) have been studied as a reagent for the dehalogenation of trichloroethylene (TCE). Ni–Fe (0.1 g) nanoparticles reduced TCE from a 40-mL saturated aqueous solution (24 ppm) to <6 ppb in 120 min. The dehalogenation reaction, based on the surface area normalized rate constant, was 50–80 times slower using nanoiron or iron filings, respectively. On the bimetallic particles, the reaction occurs by nickel-catalyzed hydrodechlorination. As the iron actively corrodes, the cathodically protected nickel surface chemisorbs hydrogen ions. TCE adsorbed to the Ni surface is thus hydrogenated. This reaction competes kinetically with the evolution of molecular hydrogen. Hydrogenation of the C–Cl bond results in the formation of linear as well as branched saturated and unsaturated hydrocarbons. The final TCE degradation products are predominantly even-numbered saturated hydrocarbons, such as butane, hexane, and octane. The toxic dehalogenation products vinyl chloride (VC), 1,1-dichloroethylene (1,1-DCE), *cis*-dichloroethylene (*cis*-DCE), and *trans*-dichloroethylene (*trans*-DCE) form only in trace amounts and do not persist. A kinetic solvent isotope effect of  $k_{\text{H}_2\text{O}/\text{D}_2\text{O}} = 14$  was observed, which indicates that C–H bond formation is rate-determining. This explains why VC and DCE, which are formed at zerovalent iron surfaces by a reaction in which electron transfer is the rate-determining step, do not accumulate. The fast reaction rate and the absence of toxic side products suggest that bimetallic nanoparticles containing good catalysts for hydrogenation (e.g., Ni, Pd, Pt) should be improved materials for the *in situ* or *ex situ* dehalogenation of chlorinated organics.

## Introduction

Recent research has focused on the development of *in situ* methods for destroying chlorinated organic molecules, such as  $\text{CCl}_4$  (carbon tetrachloride), PCE (tetrachloroethylene), and TCE (trichloroethylene), in groundwater and surface waters. A concentration of only a few parts per million (ppm) of these possible carcinogens in water supplies requires expensive pump-and-treat methods.<sup>1–4</sup> Zerovalent iron is currently employed in field studies as a permeable barrier, offering a lower cost, *in situ* alternative to the removal of chlorinated hydrocarbons. Iron has been found to degrade organohalides by reductive dehalogenation, producing relatively innocuous hydrocarbons.<sup>5–16</sup>

\* To whom correspondence should be addressed. Phone: (814) 863-9637. Fax: (814) 863-8403. E-mail: tom@chem.psu.edu.

(1) Mackay, D. M.; Cherry, J. A. *Environ. Sci. Technol.* **1989**, *23*, 630.

(2) Scherer, M. M.; Richter, S.; Valentine, R. L.; Alvarez, P. J. J. *Crit. Rev. Microbiol.* **2000**, *26* (4), 221–264.

(3) Gotpagar, E. G.; Tsang, T.; Bhattacharyya, D. *Environ. Prog.* **1997**, *16* (2), 137.

(4) Gillham, R. W.; O' Hannesin, S. F. *Groundwater* **1994**, *32* (6), 958.

(5) Rumer, R. R.; Ryan, M. E. *Barrier Containment Technologies For Environmental Remediation Applications*; Wiley & Sons: New York, 1995.

(6) Matheson, L. J.; Tratnyek, P. G. *Environ. Sci. Technol.* **1994**, *28*, 2045.

(7) Orth, S. W.; Gillham, R. W. *Environ. Sci. Technol.* **1996**, *30*, 66.

Some of the products of this reaction, such as vinyl chloride (VC), are more toxic than their parent compound (TCE) and are only slowly reduced by iron. The dehalogenation rate decreases as the number of chlorine atoms in the molecule decreases, consistent with the reduced thermodynamic driving force for electron transfer from iron to the molecule. In some applications the persistence of VC and related compounds may limit the utility of iron filings. Their presence has been reported to dictate the overall design of metal-based treatment systems.<sup>4,7–10,17</sup>

Since the dechlorination reaction of halogenated contaminants is surface-mediated, increasing the sur-

(8) Liang, L.; Korte, N.; Goodlaxson, J. D.; Clausen, J.; Fernando, Q.; Muktikian, R. *Ground Water Monit. Rem.* **1997**, Winter, 122.

(9) Arnold, W. A.; Roberts, A. L. *Environ. Sci. Technol.* **2000**, *34*, 1794.

(10) Tratnyek, P. G.; Johnson, T. L.; Scherer, M. M.; Eykholt, G. R. *Ground Water Monit. Rem.* **1997**, 108.

(11) Roberts, A. L.; Totten, L. A.; Arnold, W. A.; Burris, D. R.; Campbell, T. J. *Environ. Sci. Technol.* **1996**, *30* (8), 2654.

(12) Campbell, T. J.; Burris, D. R.; Roberts, A. L.; Wells, J. R. *Environ. Toxicol. Chem.* **1997**, *16* (4), 625.

(13) Yak, H. K.; Wenclawiak, B. W.; Cheng, I. F.; Doyle, J. G.; Wai, C. M. *Environ. Sci. Technol.* **1999**, *33*, 1307.

(14) Yak, H. K.; Lang, Q.; Wai, C. M.; *Environ. Sci. Technol.* **2000**, *34*, 2792.

(15) Casey, F. X. M.; Ong, S. K.; Horton, R.; *Environ. Sci. Technol.* **2000**, *34*, 5023.

(16) Su, C.; Puls, R. W. *Environ. Sci. Technol.* **1999**, *33*, 163.

(17) Johnson, T. L.; Scherer, M. M.; Tratnyek, P. G. *Environ. Sci. Technol.* **1996**, *30*, 2634.

face area of the iron increases the rate of reduction of TCE. The introduction of a second, catalytic metal results in an even higher dehalogenation rate.<sup>17–20</sup> Higher dehalogenation rates have already been observed for low surface area palladized iron,<sup>8,19</sup> and for high surface area particle combinations of nickel, zinc, iron, palladium, and silver.<sup>20,21</sup> High surface area nanoiron samples have been coated with palladium, and faster degradation rates have been obtained relative to nanoiron alone.<sup>22</sup> Mechanistic studies of the dehalogenation by iron have shown that the rate-determining step is electron transfer to the surface-adsorbed molecule.<sup>6</sup> This mechanism explains the slower reduction rates of DCE and VC, which are poorer electron acceptors than TCE.<sup>6</sup>

With bimetallic particles, it has been suggested that Fe or Zn acts as the reductant for water and that the second metal, Pd, Pt, Ag, or Ni, acts as a catalyst.<sup>20,21,23</sup> The introduction of a second, catalytic metal could prevent toxic byproduct formation by dehalogenating TCE via hydrogen reduction rather than via electron transfer.<sup>17,18,20,24</sup> The product ratios formed during the dehalogenation reaction have been found to be dependent on the identity of the metals employed and the concentration of hydrogen in the aqueous phase.<sup>20,25</sup>

In this study, zerovalent bimetallic nickel–iron (1:3 Ni:Fe) nanoparticles (3–30-nm diameter) were used for the dehalogenation of TCE in batch experiments. As expected, these nanoparticles offer a high surface area to volume ratio, and much higher reactivities than nanoiron or iron filings. To elucidate the improvement in dehalogenation rate and particularly in product distributions from a mechanistic standpoint, the roles that nickel and iron play in the dehalogenation of TCE were studied by measuring kinetics and product distributions in  $H_2O$  and  $D_2O$  solutions. These studies confirm the catalytic dehalogenation mechanism and explain the absence of vinyl chloride among the reaction products.

## Experimental Section

Bimetallic nanoparticles were prepared by the method described previously for nanoscale zerovalent iron.<sup>26</sup> Briefly, 12.3 g of  $FeSO_4 \cdot 7H_2O$  [44 mmol] (Aldrich) and 3.0 g of  $NiCl_2 \cdot 6H_2O$  [12.6 mmol] (Aldrich) were dissolved in 100 mL of Nanopure (18.3 M $\Omega$ -cm) water with stirring. After the pH was adjusted to 6.2–7.0 with 3.8 M NaOH, the salts were reduced to black particles using 6.0 g of  $NaBH_4$  [158 mmol] (Aldrich). The same method was used to synthesize the nanoscale nickel and nanoscale iron particles separately, with the weight ratio of metal to borohydride adjusted appropriately. No special precautions were taken to eliminate oxygen from the reaction vessel. The mixture was allowed to stir for 20 min and was

then filtered as previously described.<sup>26</sup> After filtration, washing with water, and then washing with ethanol and acetone to eliminate water, the particles were dried in a vacuum oven.

Palladium-coated nanoiron (Pd–Fe) particles were synthesized according to the procedure described by Zhang et al.<sup>20</sup> The nanoiron was first prepared by borohydride reduction using 6.2 g of  $FeSO_4 \cdot 7H_2O$  (Aldrich) in 100 mL of deionized water (pH adjusted to 6.2–7.0, as described above) and reduced with 3.1 g of  $NaBH_4$  (Aldrich). The iron nanoparticles were then filtered, washed with water, and then immediately suspended in 0.1 g of palladium(II) acetate  $[Pd(C_2H_3O_2)_3]$  in 20 mL of ethanol. Afterward, the palladium-coated nanoiron particles were vacuum-filtered, washed with ethanol and acetone, and finally dried in a vacuum oven overnight.

The iron filings used for comparisons of the dehalogenation rates and characterization results were obtained from Fisher (40 mesh) and were used as received.

**Physical Characterization.** X-ray powder diffraction (XRD) was performed using a Philips X'Pert MPD diffractometer. X-ray photoelectron spectroscopy (XPS) was performed on a Kratos XSAM800 pci. Nitrogen Brunauer–Emmet–Teller (BET) surface area analysis was performed using a Micromeritics ASAP 2010. Iron, nickel, and boron bulk content were determined using a Leeman Labs PS3000UV inductively coupled plasma spectrophotometer (ICP-AES) at the Penn State Materials Characterization Laboratory. In each case, 0.1 g of sample was digested in a minimum amount of concentrated HCl, and the solution was diluted with deionized water to 100.0 mL for ICP analysis. The final solution contained about 5 wt % acid. Thermogravimetric analysis (TGA) was performed to determine the oxide content of the nanoparticles using a TA Instruments Thermogravimetric Analyzer (TGA 2050). TGA experiments were run in air, heating at a rate of 5 °C/min to 1000 °C. Transmission electron microscope (TEM) images were obtained on a JEOL 1200EXII microscope at the electron microscope facility for the Life Sciences in the Biotechnology Institute at The Pennsylvania State University.

**Batch Experiments Using TCE.** To evaluate the reactivity of the nanoscale particles, batch experiments were performed in which the removal of  $1.8 \times 10^{-4}$  M TCE (Aldrich 99.5%) from Nanopure (18.3 M $\Omega$ -cm) water was monitored.

Generally, 0.1 g of unsupported Ni–Fe nanoparticles was weighed into a 40-mL IC Chem vial (VWR) with a Teflon minimert valve or a Teflon–Silicon septum.  $1.8 \times 10^{-4}$  M aqueous TCE was added to the vials. For purge and trap sampling, the vials were filled completely with solution to eliminate all headspace, whereas for headspace sampling 10 mL of headspace remained. No precautions for oxygen elimination from the vials or from the solution were taken. The reaction vials were rotated on a roller drum at 11 rpm, with their axis in the horizontal position, at ambient temperature. For purge and trap analysis, 5.0 mL of the aqueous phase was withdrawn by a gastight syringe (Hamilton) and injected directly into the purge and trap vessel.

A purge and trap apparatus, used to preconcentrate and separate the organics from the aqueous phase (Tekmar LCS-2), was coupled to a gas chromatograph (Buck Scientific) equipped with a Restek MXT-502.2 60-m column and a dry electrolytic conductivity (DELCD) detector. The sample was purged for 8 min in a water bath kept at a constant temperature of 35 °C and then desorbed for 5 min at 180 °C. The temperature program for the GC was 40 °C for 5 min, followed by a ramp at 10 °C/min to 200 °C. The carrier gas was helium.

To determine if a significant amount of TCE was sorbed to the Ni–Fe nanoparticles, the total concentration of TCE in the vial and the aqueous concentration of TCE were also determined by purge and trap. We added 0.1 g of NiFe nanoparticles to a 40-mL vial filled with  $1.8 \times 10^{-4}$  M TCE solution. In 30-min intervals, samples were split into fractions for either ICP analysis (for nickel and iron concentration) or purge and trap analysis (for total and aqueous TCE concentration). An 8-mL fraction for the analysis of iron and nickel ions by ICP-AES was first passed through a 0.02- $\mu$ m membrane filter (Whatman). From the remaining 32 mL of TCE solution containing the Ni–Fe nanoparticles, 16 mL of the aqueous

(18) Gotpagar, J.; Lyuksyutov, S.; Cohn, R.; Grulke, E.; Bhattacharya D. *Langmuir* **1999**, *15*, 8412.

(19) Li, T.; Farrell, J. *Environ. Sci. Technol.* **2000**, *34*, 173.

(20) Zhang, W.-X.; Wang, C.-B.; Lien, H.-L. *Catal. Today* **1998**, *40*, 387.

(21) Li, W.; Klabunde, K. J. *Croat. Chem. Acta* **1998**, *71* (4), 853.

(22) Wang, C.-B.; Zhang, W.-X. *Environ. Sci. Technol.* **1997**, *31* (7), 2154.

(23) Nyer, E. K.; Vance, D. B. *Ground Water Monit. Rem.* **2001**, Spring, 41.

(24) Li, T.; Farrell, J. *Environ. Sci. Technol.* **2000**, *34*, 173.

(25) Lowry, G. V.; Reinhard, M. *Environ. Sci. Technol.* **2000**, *34*, 3217.

(26) Ponder, S. M.; Darab, J. G.; Mallouk, T. E. *Environ. Sci. Technol.* **2000**, *34*, 2564.

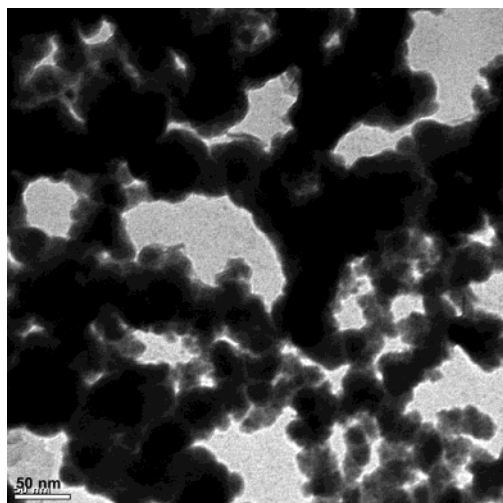


**Figure 1.** Transmission electron microscopy image of Ni-Fe nanoparticles.

fraction was withdrawn and analyzed by purge and trap/GC for TCE removal. The Ni-Fe nanoparticles plus 16 mL of TCE solution were analyzed for total TCE concentration by the same method. This experiment was carried out with many identical vials so that a new vial could be sampled at each 30-min interval, to follow the time course of TCE adsorption and reduction.

The products formed during the dehalogenation reaction were monitored by headspace-GC/MS analysis. For the headspace sampling, 0.5 mL of headspace gas was introduced by splitless injection into the GC/MS at a 200 °C injector temperature using a Hewlett-Packard 5972 GC/MS with a 30-m GasPro column (J&W).

The program was 40 °C for 1 min, followed by a ramp at 5 °C/min to 200 °C. After each headspace sample was removed, 0.5 mL of argon was injected to keep the internal pressure in the vial constant.

The procedure used to determine the amount of hydrogen produced from the nanoparticles was identical to the headspace analysis. The analysis was carried out in deoxygenated water using a Varian aerograph GC equipped with a packed 13X molecular sieve column and a thermal conductivity (TCD) detector sensitive to the amount of oxygen, nitrogen, and hydrogen gas in the headspace. The reaction vials filled with nanoparticles were carefully purged with argon through the septa to eliminate oxygen. The chloride ion concentration was determined by means of a chloride ion selective electrode (Cole-Parmer). The change in the pH was determined at the same time as the chloride ion concentration by keeping separate chloride ion and pH sensitive electrodes attached to their meters in the vial.

## Results and Discussion

### Characterization of Bimetallic Nanoparticles.

The transmission electron micrograph (TEM) in Figure 1 shows the as-prepared unsupported Ni-Fe nanoparticles. The particles are in the range of 3–30 nm in diameter and form chains of beads. This type of aggregation has been previously attributed to magnetic interactions between the primary metal particles.<sup>27</sup> It has been suggested previously that the porous, nanocrystalline morphology results in high levels of stepped surfaces that increases their reactivity.<sup>22</sup> X-ray diffraction line widths were used to determine particle grain sizes. X-ray patterns of separately reduced Ni and Fe samples indicate crystallite diameters of 3–5 and 10–

**Table 1. Apparent Surface Compositions of Fe, Ni, and Ni-Fe Materials, Expressed as wt %, from X-ray Photoelectron Spectroscopy**

material	% Fe	% Ni	% O	% B	% Na	% C
iron filings	30.1		29.5			40.4
nanoiron	41.6		44.0	11.4	3.08	0.0
nanonickel		45.7	35.7	10.9	0.94	6.89
Ni-Fe	34.8	5.63	41.5	8.29	1.10	8.73

**Table 2. ICP-AES Analytical Data for Iron Filings, Nanoiron, Nanonickel, Nano-nickel-iron (Ni-Fe) Reduced Simultaneously in a 1:3.7 Mass Ratio and a Physical Mixture (Ni:Fe) of Nanoiron and Nanonickel**

material	% Fe	% Ni	% B
iron filings	94.3		
nanoiron	83.0		4.2
nanonickel		73.0	6.9
Ni-Fe	53.1	15.6	5.3
Ni:Fe mixture	63.3	18.6	6.2

**Table 3. BET Surface Areas and TCE Remediation Rates for Fe, Ni, Ni-Fe, and Ni:Fe Materials**

material used	BET surface area (m <sup>2</sup> /g)	TCE decomposition rate (h <sup>-1</sup> )	surface area normalized rate (L h <sup>-1</sup> m <sup>-2</sup> )
Ni:Fe 50:50	0.49	no change after 4 days	
iron filings	2.6	0.0078	(1.2 ± 0.4) × 10 <sup>-3</sup>
nanoiron	18	0.09	(2.0 ± 0.1) × 10 <sup>-3</sup>
nanonickel	35	0.14	(8.0 ± 1.0) × 10 <sup>-3</sup>
Ni-Fe	59	13.7	(9.8 ± 0.7) × 10 <sup>-2</sup>
physical mixture	25	3.0	(5.4 ± 0.9) × 10 <sup>-2</sup>
Ni:Fe			

30 nm, respectively. To gain more insight into the nature of the phases present, the composite was heated in an argon atmosphere to 450 °C, which sharpened the X-ray reflections. Sharper reflections corresponding to body-centered-cubic (bcc) Fe and face-centered cubic (fcc)  $\gamma$ -Fe<sub>x</sub>Ni alloy (which can be distinguished from fcc Ni by its lattice constant) were then observed. Ni has limited solubility in Fe, and the observation of separate phases upon heating is consistent with the equilibrium phase behavior of the system. The lattice constant (3.585 Å) of the  $\gamma$ -Fe<sub>x</sub>Ni phase made by heating to 450 °C corresponds to about 40% Ni content, consistent with the phase diagram of bulk Ni and Fe.<sup>28</sup> The fact that the fcc Ni lines are much broader than those of bcc Fe when the individual metals are precipitated by borohydride reduction suggests a structural model for the as-prepared material in which very small Ni-rich grains are intimately mixed with 10–30-nm bcc Fe grains.

Consistent with the small particle size and porous morphology, the Ni-Fe material has a BET surface area of 59 m<sup>2</sup>/g (Table 3). X-ray photoelectron spectra (XPS) (Table 1) and ICP-AES (Table 2) data showed that the particles retained a significant amount of boron from the borohydride reduction and that the surface (within the 1–2-nm sampling depth of XPS) was enriched in both oxygen and iron. Both the surface boron and iron atoms were oxidized, as determined from the B 1s and Fe 2p<sub>1/2</sub> binding energies of 192 and 712 eV, respectively. The mass ratio of Fe to Ni in the solution used to prepare the particles was 3.7, and the analytical ratio in the product (Table 2) was 3.4.

(28) Okamoto, K., Ed.; *Phase Diagrams of Binary Iron Alloys*; ASM International: Materials Park, OH, 1993; pp 263–264.

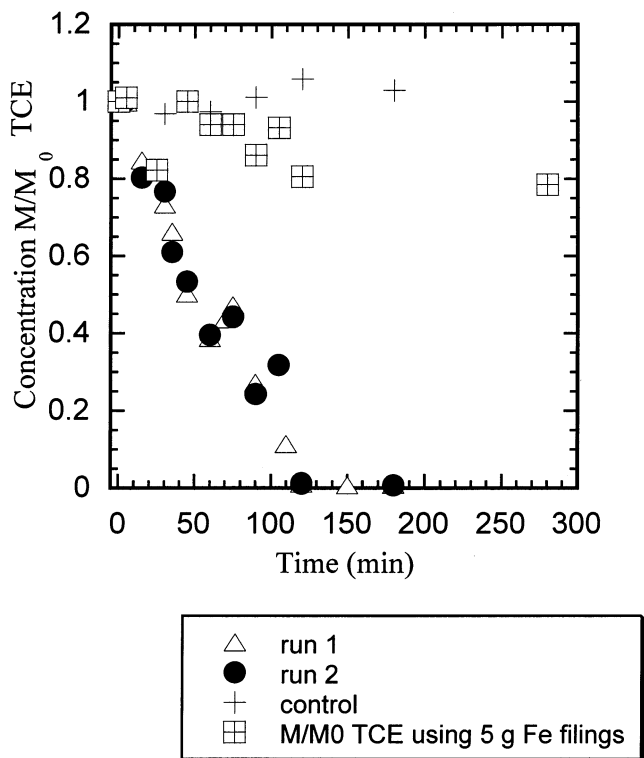


**Figure 2.** Dehalogenation of 40-mL aqueous  $1.8 \times 10^{-4}$  M TCE using 0.1 g of Ni-Fe nanoparticles and 5 g of iron filings. The circles and triangles show duplicate runs with 0.1 g of Ni-Fe, the squares 5 g of iron fillings, and plus signs control using TCE without Fe.

The oxide content was determined by comparing TGA runs with Ni-Fe particles exposed to the atmosphere used in the experiments, and Ni-Fe particles reduced in hydrogen at 300 °C for 3 h to ensure near zero initial oxide content. TGA analysis of the Ni-Fe particles gave a bulk oxide content of about 7%, meaning that the core of the particles contains zerovalent iron. This is lower than the surface value determined by XPS, consistent with the idea that most of the oxide is concentrated on the surface of the nanoparticles.

**Dehalogenation of TCE.** Figure 2 shows data for the dehalogenation of  $1.8 \times 10^{-4}$  M (23.4 ppm) TCE with 0.1 g of Ni-Fe nanoparticles (duplicate runs), and as a comparison with 5 g of iron filings. Within 120 min, TCE was reduced below the detection limit of the detector, which was  $5 \times 10^{-8}$  M (6 ppb).

Several other nickel- and iron-based powders were tested for TCE dehalogenation: nanoiron and nanonickel reduced separately, a mixture of the separately reduced nanoiron and nanonickel particles (analytical mass ratio of 3.4:1), and a commercial Ni-Fe alloy of 50:50 ratio (Alfa Aesar, 100 mesh). The TCE decay curves were fitted to a single exponential to obtain the pseudo-first-order rate constant,  $k_{\text{obs}}$ . From eqs 1 and 2, the BET surface area, and the vial loadings in g of Fe/L for each sample, the surface area normalized rate constant can be calculated. Here,  $\rho_a$  is the surface area concentration of  $\text{Fe}^0$  in  $\text{m}^2/\text{L}$  of solution,  $k_{\text{obs}}$  is the

$$-\frac{d[P]}{dt} = k_{\text{SA}}\rho_a[P] \quad (1)$$

$$k_{\text{SA}} = k_{\text{obs}}/\rho_a \quad (2)$$

pseudo-first-order rate constant in  $\text{h}^{-1}$ , and  $[P]$  is the concentration of the reacting halocarbon.<sup>17</sup> When dehalogenation rates are characterized by  $k_{\text{SA}}$ , the rate is independent of the mass, surface area of the metal, and volume of reaction system used.

From the BET surface areas, one expects the high surface area nanoiron to dehalogenate TCE faster than iron filings. This trend is observed for the pseudo-first-order rate constants, where nanoiron reduces TCE 11 times faster than do iron filings. Once the surface area is taken into account by calculating  $k_{\text{SA}}$ , the normalized rate is only increased by a factor of 1.6. The most striking difference in surface normalized rate is between the bimetallic particles and nanoiron or iron filings. Both nanoiron and iron filings required several days to degrade TCE to a 5 ppb concentration. Fitting the TCE decay curve to a single exponential, nanoiron had a surface area normalized dehalogenation rate of  $2.0 \times 10^{-3}$   $\text{L h}^{-1} \text{m}^{-2}$ , and iron filings had a rate of  $1.2 \times 10^{-3}$   $\text{L h}^{-1} \text{m}^{-2}$ , compared to  $9.8 \times 10^{-2}$   $\text{L h}^{-1} \text{m}^{-2}$  for Ni-Fe. This clearly shows that the addition of a hydrogenation catalyst has a tremendous effect on the dechlorination rate. Palladium-coated nanoiron synthesized as described by Zhang et al.<sup>20</sup> reduced  $1.8 \times 10^{-4}$  M TCE in 5–10 min (measured with our analytical apparatus), which translates to  $k_{\text{obs}} = 43 \text{ h}^{-1}$  or  $k_{\text{SA}} = 5.7 \times 10^{-1}$   $\text{L h}^{-1} \text{m}^{-2}$ , that is, about 9 times faster than the Ni-Fe nanoparticles. This difference reflects more efficient catalysis of the hydrogenation reaction by Pd, which is known to be a better catalyst than Ni. Consistent with observations by Zhang et al., the powders tested that contained only iron had slow dehalogenation rates.

A physical mixture of nanoiron and nanonickel, in which the metal salts were reduced separately and then mixed in a 1:3.4 Ni-Fe ratio, also had faster dehalogenation rates than nanoiron, but was slower than Ni-Fe reduced together. This observation is consistent with the idea that nickel and iron need to be in electronic contact in order for catalysis to occur. The bimetallic particles effectively form a galvanic cell, in which Fe passes electrons to the catalytic metal, where TCE is reduced. Nanonickel alone was a poor reagent for the dehalogenation of TCE. After 3.5 h of reaction with 0.5 g of nanonickel, 80% of the TCE was still present in the suspension. As another comparison, a commercial mixture of sintered Ni:Fe powder was also used to dehalogenate TCE. After 4 days of exposure none of the TCE had been removed.

Sorption of TCE to nonreactive sites has been previously observed with iron filings, and we analyzed our samples to determine if sorption was a significant factor in the removal of TCE from the test solutions.<sup>29</sup> After calculation of the difference between total TCE concentration in the vial (metal plus aqueous fraction) and the aqueous TCE concentration as a function of time, no significant TCE concentration differences between the two were observed for Ni-Fe nanoparticles, meaning that significant sorption is not responsible for TCE disappearance.

In the course of the dehalogenation reaction, the pH increased from 8.4 to 9.6, and  $\sim 9.0 \times 10^{-5}$  M chloride ions were released. Assuming that for each degraded

(29) Burris, D. R.; Campbell, T. J.; Manoranjan, V. S. *Environ. Sci. Technol.* **1995**, 29, 2850.

TCE molecule three chloride ions are produced, the chloride ion formation was not quantitative and amounts to about 17% chloride ion recovery. Lower chloride concentrations may be explained by the formation of insoluble chloride-containing iron hydroxides (green rusts), or adsorption of chloride by the metal corrosion products. In 120 min, the amount of oxidized iron formed was 2% of the initial amount of iron. No nickel ions could be detected during this short time period. ICP analyses were done over a period of 33 days with vials loaded with 0.1 g of samples of nanoiron, nanonickel, or Ni–Fe in 40.0 mL of TCE solution. The final metal ion concentrations resulting from dissolution were 29 ppm for nanoiron, 13 ppm for nanonickel, and 4.3 ppm Fe and 0.04 ppm Ni (detection limit for Ni is 0.02 ppm) for Ni–Fe. This shows that when nickel and iron are reduced together, forming electronic contact, the iron oxidizes whereas the nickel oxidation is inhibited. It is surprising that iron dissolution is faster in the absence of nickel since one expects iron corrosion to increase when a catalytic metal is added. While Ni is cathodically protected by Fe over the time scale of this experiment, it is likely that when all the iron is spent, nickel corrosion will occur. Long-term studies using Ni–Fe would be needed to quantify possible leaching of nickel ions, especially once all the iron has been corroded.

To determine the solid product phases formed from Ni–Fe during the dehalogenation reaction, powder X-ray diffraction (XRD) experiments were carried out on samples exposed to TCE for 30 and 105 min. The XRD patterns showed the progressive growth of broad peaks assigned to magnetite ( $Fe_3O_4$ ), in addition to residual body-centered cubic iron.<sup>30</sup> The crystallite size of magnetite determined from the X-ray diffraction line width was 6–15 nm. This does not exclude the possible formation of other product phases that are either amorphous or composed of particles too small to be detected by XRD.

**Hydrogen Formed from Water Reduction Initiated by Metal Particles.** To test the galvanic cell hypothesis, the initial rates of hydrogen generation from 0.1 g of nano-Ni–Fe, nanoiron, nanonickel, and a 3:4:1 physical mixture of nanoiron and nanonickel in deoxygenated water were compared (Figure 3A). Because of the low concentration of TCE in water, these rates did not differ if water was substituted by saturated TCE solution. Large amounts of hydrogen gas are generated only with nano-nickel–iron reduced together, supporting a bipolar reaction mechanism in which nickel and iron need to be in electronic contact for high activity.

The initial hydrogen evolution rate provides a measure of the anaerobic corrosion rate, but caution should be used in extrapolating these data to nanoparticle lifetimes.<sup>31</sup> This high initial corrosion rate is a consequence of the fact that the iron surface is initially nonpassivated. The initial rate for Pd-coated nanoiron (0.105  $\mu\text{mol}/\text{min}$ ) is significantly higher than that for Ni–Fe nanoparticles (0.025  $\mu\text{mol}/\text{min}$ ). The fact that the better hydrogen evolution catalyst gives a higher rate

(30) While it is difficult to distinguish magnetite ( $Fe_3O_4$ ) from maghemite (cubic  $Fe_2O_3$ ) by powder X-ray diffraction, particularly with small particles, it is known that  $Fe(OH)_2$  is converted to magnetite under the conditions of our experiments (Schikorr, G. Z. Z. *Electrochim. 1929*, 35, 62).

(31) Reardon, E. J. *Environ. Sci. Technol.* **1995**, 29, 2936.

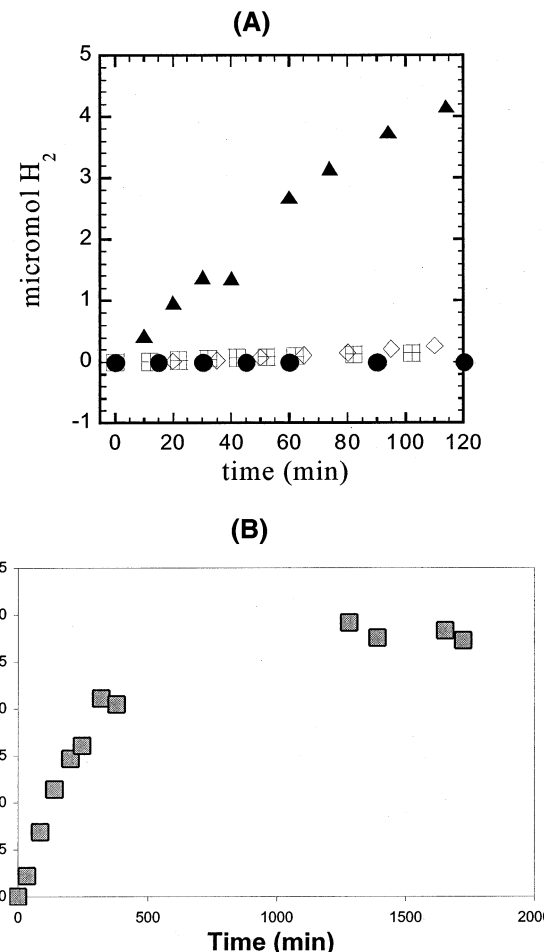


**Figure 3.** (A) Comparison of the amount of hydrogen gas ( $\mu\text{mol}$ ) produced by reaction with water, measured by static headspace analysis (1.0 mL of headspace sampled, 0.1 g metal loading in 40 mL vials). When iron and nickel are reduced together, a galvanic couple is formed and water is reduced to hydrogen. The squares represent nanoiron, the circles nanonickel, the tilted squares a physical mixture of nanonickel and nanoiron (Ni:Fe), and the triangles nano-Ni–Fe reduced together (Ni–Fe). (B) Amount of hydrogen gas ( $\mu\text{mol}$ ) produced by Ni–Fe nanoparticles in water at longer exposure times. The static headspace was analyzed as described for Figure 3A. The hydrogen evolution reaches a steady state at longer exposure times and does not increase at a linear rate.

means that the initial corrosion process is cathodically controlled. A study run for 30 h using Ni–Fe nanoparticles (Figure 3B) showed that the rate of hydrogen evolution is roughly constant during the first 5 h and then slows down markedly as the reaction shifts to anodic control. By sampling the headspace and then purging the vial with Ar once per day, it was determined that the hydrogen generation rate remained constant for 7 days at 3  $\mu\text{mol}/\text{day}$ . If this rate of hydrogen production is maintained until all of the 0.95 mmol of  $Fe^0$  contained in 0.1 g of Ni–Fe are converted to  $Fe^{2+}$ , then the lifetime of these particles would be approximately 300 days. As the iron is oxidized, protons from water are reduced to adsorbed hydrogen atoms and molecular hydrogen. The hydroxyl ions produced react directly with  $Fe^{2+}$  ions to make an oxide precipitate. Longer term studies are needed to fully investigate iron passivation during corrosion, particularly in solutions containing sulfate, bicarbonate, and chloride that more accurately simulate groundwater.

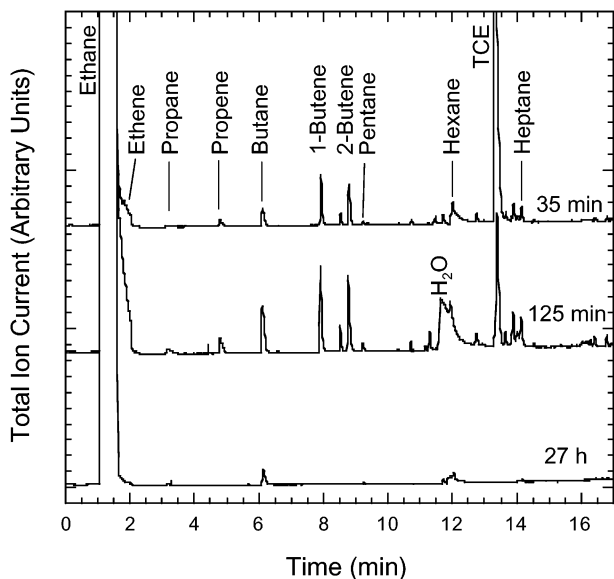


**Figure 4.** GC/MS total ion chromatograms obtained from 1.0 mL of headspace, using 0.1 g of Ni–Fe in aqueous TCE solution. Top (a) = 35 min of exposure; middle (b) = 125 min; bottom (c) = 27 h.

**Reduction Products from Ni–Fe in  $\text{H}_2\text{O}$ .** To establish more definitively the mechanism of TCE dehalogenation using Ni–Fe nanoparticles, qualitative headspace analysis of the reaction products was done at 30-min intervals. Ethylene and butene were identified as the dominant reduction products in the early stage of the reaction (Figure 4, top (a) 35 min). From reconstructed ion chromatograms of the appropriate molecular masses, VC and DCE can be extracted from the baseline signal. Trace amounts of halogenated products, mainly *cis*-DCE and 1,1-DCE, were also detected. As the reaction progressed, more branched and straight-chain alkanes (C1–C8) were formed in addition to olefins (Figure 4, middle (b) 125 min). After a much longer time the alkenes were fully reduced and the predominant alkane products were even-numbered: butane, hexane, and octane (Figure 4, bottom (c) 27 h). At this stage of the reaction, no TCE or chlorinated products remained. The carbon recovery based on the GC results after 27 h was calculated from the initial TCE concentration using Henry's law. The recovery was 92%. Some loss of volatile alkane products can be attributed to a pressure increase in the vials and can account for the observed losses.

Since ethylene is a likely intermediate in the reaction, ethylene was purged through 0.1 g of nano-Ni–Fe in water for 30 min. Ethane was produced at first, but then larger amounts of C3–C6 hydrocarbons were observed. Interestingly, fewer different hydrocarbon products were formed from ethylene than from TCE. It is possible that the C–C bond is more easily broken when a chlorinated compound is reductively adsorbed. This idea is supported by the fact that when *trans*-DCE or VC was added to Ni–Fe, dichloromethane was detected. Pd-coated nanoiron produced only even-numbered carbon hydrogenation products, consistent with previous findings,<sup>21,25</sup> showing that Ni catalyzes C–C bond breaking whereas Pd does not. Branched hydrocarbons are observed with Ni, but are not major products. Branching

may indicate that hydride and methyl migrations occur on the nickel surface, implying radical intermediates. Previously, Li and Klabunde also observed monocarbon species when studying the dehalogenation of TCE on palladium-doped zinc particles, and Fennelly and Roberts suggested the formation of radicals and carbenoids as possible intermediates with bimetallic reductants.<sup>21,32</sup> The change in product distribution might also be attributed to a change in the hydrogen concentration, as was observed by Lowry and Reinhard, who found fewer radical coupling products with increasing hydrogen concentration using a palladium catalyst.<sup>25</sup>

Similar experiments using iron filings and nanoiron produced ethene, propene, butane, and butenes. Iron filings and nanoiron also produced VC, 1,1-DCE, *trans*- and *cis*-DCE in detectable amounts, and these intermediates were still present after 70 h of exposure. Previous studies detected alkanes when iron filings were exposed to water or chlorinated organics, and postulated that alkanes were formed either from  $\text{CO}_2$  dissolved in water or from carbide impurities in the iron.<sup>33,34</sup> Control experiments using Ni–Fe in water without TCE did not produce any alkanes, meaning that these sources of carbon were not significant contributors to the products observed in our experiments.

**Reduction Products from Ni–Fe in  $\text{D}_2\text{O}$ .** As a further semiquantitative test of the hydrodechlorination reaction mechanism, the same dehalogenation headspace experiment was carried out in  $\text{D}_2\text{O}$ . All products had the same retention times regardless of whether water or  $\text{D}_2\text{O}$  was used as the solvent, and deuterated hydrocarbons were identified by GC/MS. The product distributions were similar to those found in  $\text{H}_2\text{O}$ , except that the appearance of saturated alkanes occurred more slowly.

The rates of TCE removal were compared in  $\text{H}_2\text{O}$  and  $\text{D}_2\text{O}$ , and an isotope effect  $k_{\text{H}}/k_{\text{D}}$  of 14 was observed. This is a very large effect, considering that a value of 7 is the semiclassical limit for hydrogen transfer from a metal surface to carbon.<sup>35</sup> Possible explanations for this large value are the influence of a thermodynamic isotope effect, or complex reaction mechanisms, in which there is a common intermediate for H/D exchange and hydrogenation, or in which quantum tunneling contributes to the rate-determining step.<sup>35</sup> The presence of perdeuterated hydrocarbons among the products provides clear evidence for H/D exchange occurring simultaneously with hydrodechlorination. For example, the most abundant butane products formed in  $\text{D}_2\text{O}$  are  $\text{C}_4\text{H}_2\text{D}_8$ ,  $\text{C}_4\text{H}_2\text{D}_9$ , and  $\text{C}_4\text{D}_{10}$ . While  $\text{C}_4\text{H}_2\text{D}_8$  could be formed from two TCE molecules without H/D exchange, the latter two must be H/D exchange products. The ratio of these three products is approximately 1:1.3:1, indicating that hydrogenation and H/D exchange have roughly comparable rates. This large H/D isotope effect is inconsistent with outer-sphere electron transfer as the rate-determining step in the reaction. The isotope data strongly

(32) Fennelly, J. P.; Roberts, A. L. *Environ. Sci. Technol.* **1998**, 32, 1980.

(33) Hardy, L. I.; Gillham, R. W. *Environ. Sci. Technol.* **1996**, 30, 57.

(34) Deng, B.; Campbell, T. J.; Burries, D. R. *Environ. Sci. Technol.* **1997**, 31, 1185.

(35) Kresge, A. J.; O'Ferrall, R. A. M.; Powell, M. F. In *Isotopes in Organic Chemistry*; Bunzel, E., Lee, C. C., Eds.; Elsevier: Amsterdam, 1976; Vol. 7, pp 177–274.

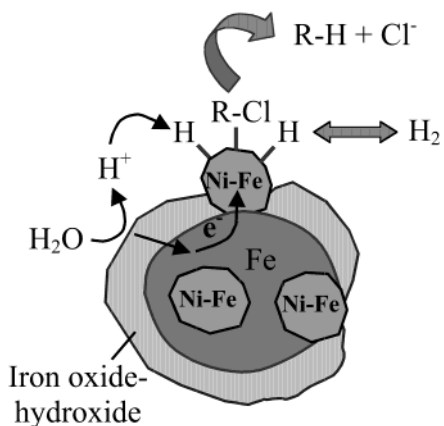


**Figure 5.** Proposed mechanism for TCE dehalogenation using nickel–iron nanoparticles. Iron corrodes, transferring electrons to Ni-rich catalytic regions of the nanoparticles, which reductively adsorb hydrogen ions. The C–Cl bond of an adsorbed TCE molecule is broken and hydride transfer occurs. Molecular hydrogen is also evolved at the Ni-rich areas of the surface.

support the idea that C–H bond formation is the rate-determining step in the Ni-catalyzed reaction.

**Catalytic Dechlorination of TCE.** The current model (Figure 5) for the dehalogenation reaction using Ni–Fe nanoparticles involves the oxidation of iron to galvanically protect the more noble nickel.<sup>20,22</sup> As iron corrodes, protons from water are reduced to adsorbed H atoms and to molecular hydrogen at the catalytic Ni surface. TCE is adsorbed onto the surface of the Ni–Fe particles where the C–Cl bond is broken, and the chlorine atom is replaced by hydrogen (Figure 5). A similar mechanism was proposed by Cheng et al. for the dehalogenation of 4-chlorophenol to phenol at palladized graphite and iron electrodes,<sup>36</sup> and by Dabro et al. for dehydrochlorination of pentachlorophenol to phenol or cyclohexanol at supported palladium electrodes.<sup>37</sup> Both used electrolysis to determine the mechanism. Other studies using granular or micrometer-sized bimetallic particles have proposed a similar mechanism.<sup>8,21</sup> These findings were further confirmed by studies carried out with nanoscale iron–palladium or platinum combinations.<sup>20,23</sup>

Interestingly, the addition of 5% Pb(NO<sub>3</sub>)<sub>2</sub> or HgNO<sub>3</sub> prior to borohydride reduction, which produced Ni–Fe–(Pb or Hg) nanoparticles, did not poison the catalytic hydrogenation reaction of nano-Ni–Fe particles. Similarly, the chloride evolved in the reaction does not appear to poison the catalyst. For practical applications, it would be useful to evaluate the possible deactivation of Ni–Fe and Pd–Fe by H<sub>2</sub>S since sulfur in mineral phases could be liberated under the reducing conditions generated by the nanoparticles.

One question in these studies concerns the role of hydrogen (produced in the corrosion reaction) in the reduction of TCE. Tests in which 0.1 g of Ni–Fe in TCE solution was respiked with TCE over a period of 14 days, completing 18 cycles, showed no decrease in activity. Over the course of 14 days, 67 μmol of H<sub>2</sub> gas was collected from 0.95 mmol of iron and a total of 190 μmol

of TCE was removed. The total amount of hydrogen evolved in this experiment was consistent with the rate observed in pure water over 7 days. This comparison indicates that the gaseous hydrogen retained in the reaction vial does not significantly assist in the catalytic dehalogenation of TCE. This is important because in a reactive barrier or direct injection application, the generated hydrogen would be free to diffuse away from the catalytic particles.

Palladium-coated nanoiron, which reduces TCE faster and has a higher initial corrosion rate than nano-Ni–Fe, showed no decrease in activity when re-spiked in the same way with TCE. Hydrogen gas (254 μmol) was detected from 1.38 mmol of iron, and 190 μmol of TCE was removed in 14 days/18 cycles by 0.1 g of palladium-coated nanoiron. Most of the hydrogen evolved during the first 7 days. The hydrogen generation rate slowed and became comparable to that of Ni–Fe at longer times. This is again consistent with anodic control of the reaction as the iron surface becomes passivated.

## Conclusions

By analyzing the solid and aqueous products formed during the dehalogenation reaction, we have confirmed that bimetallic nanoparticles react through a bipolar mechanism, in which iron corrodes as the second metal catalyzes the reduction of chlorinated hydrocarbons. The bipolar mechanism is supported by the fact that a physical mixture of Ni and Fe shows much slower reaction with TCE and slower corrosion. Both the product distribution and the H/D isotope effect strongly support the idea that Ni acts as a hydrogenation catalyst in the case of Ni–Fe nanoparticles. An important consequence of this catalysis is that DCE and VC, which are much more slowly reduced than TCE at iron surfaces, are rapidly hydrogenated at Ni and therefore do not accumulate in the reaction. Even though leaching of nickel from the Ni–Fe nanoparticles was not observed over a 33-day time period, it still might be of environmental concern for long-term burial where nickel leaching occurs once the iron has been exhausted. This suggests that palladium, being more stable than nickel, would be a better choice of catalyst for most applications.

However, because the second metal catalyzes both the hydrogenation reaction and the evolution of molecular hydrogen, the initial corrosion rate increases when a more active catalyst, such as Pd, is used. As the iron surface becomes passivated and the reaction shifts to anodic control, the difference between catalytic metals becomes less pronounced. Because of background corrosion, the useful lifetime of zerovalent metal nanoparticles will be more limited than that of lower surface area iron. Anaerobic corrosion rates measured over a 7-day period gave an extrapolated lifetime of 300 days for Ni–Fe. Thus, it appears that Ni–Fe and Pd–Fe nanoparticles are more suitable for shorter term remediation applications, such as injection into contaminated groundwater than in reactive barriers that are intended to remain active for years or decades. By varying the ratio of Fe to catalytic metal, or by supporting or encapsulating these nanoparticles, it may be possible to change the corrosion rate while retaining the appropriate degree of reactivity for a particular environmental application.

(36) Cheng, I. F.; Fernando Q.; Korte, N. *Environ. Sci. Technol.* **1997**, *31*, 1074.

(37) Dabro, P.; Cyr, A.; Laplante, F.; Jean, F.; Menard, H.; Lessard, J. *Environ. Sci. Technol.* **2000**, *34*, 1265.

**Acknowledgment.** This work was supported by the U.S. Department of Energy under Contract DE-FG07-97ER14822. We thank Henry Gong for performing the ICP-AES analyses and Dr. Rosemary Walsh and the Electron Microscope Facility for the Life Sciences in the

Biotechnology Institute at The Pennsylvania State University for the use of the transmission electron microscope.

CM020737I